Cancer Cell
Article

A Perivascular Niche for Brain Tumor Stem Cells

Christopher Calabrese,[1] Helen Poppleton,[1] Mehmet Kocak,[2] Twala L. Hogg,[1] Christine Fuller,[3] Blair Hamner,[4] Eun Young Oh,[1] M. Waleed Gaber,[5] David Finklestein,[6] Meredith Allen,[1] Adrian Frank,[1] Ildar T. Bayazitov,[1] Stanislav S. Zakharenko,[1] Amar Gajjar,[7] Andrew Davidoff,[4] and Richard J. Gilbertson[1,7,*]
[1] Department of Developmental Neurobiology
[2] Department of Biostatistics
[3] Department of Pathology
[4] Department of Surgery
[5] Department of Radiation Oncology
[6] The Hartwell Center for Bioinformatics and Biotechnology
[7] Department of Oncology
St. Jude Children's Research Hospital, 332 North Lauderdale Street, Memphis, TN 38105, USA
*Correspondence: richard.gilbertson@stjude.org
DOI 10.1016/j.ccr.2006.11.020

SUMMARY

Cancers are believed to arise from cancer stem cells (CSCs), but it is not known if these cells remain dependent upon the niche microenvironments that regulate normal stem cells. We show that endothelial cells interact closely with self-renewing brain tumor cells and secrete factors that maintain these cells in a stem cell-like state. Increasing the number of endothelial cells or blood vessels in orthotopic brain tumor xenografts expanded the fraction of self-renewing cells and accelerated the initiation and growth of tumors. Conversely, depletion of blood vessels from xenografts ablated self-renewing cells from tumors and arrested tumor growth. We propose that brain CSCs are maintained within vascular niches that are important targets for therapeutic approaches.

INTRODUCTION

There is now compelling evidence that the bulk of the malignant cells in cancers are generated by rare fractions of self-renewing, multipotent, and tumor-initiating cells, termed cancer stem cells (CSCs) (Al-Hajj et al., 2003; Lapidot et al., 1994; Singh et al., 2004). Whether CSCs arise from normal stem cells or more differentiated cells is not known. Nevertheless, CSCs resemble the normal stem or progenitor cells of the corresponding tissue of origin. For example, brain CSCs express CD133 and Nestin that mark neural stem and progenitor cells (Galli et al., 2004; Singh et al., 2004; Taylor et al., 2005), and we recently reported that CSCs isolated from ependymomas are remarkably similar to radial glia that are neural precursor cells (Taylor et al., 2005).

If tumors are derived entirely from CSCs, then drugs that kill these cells could prove highly effective treatments of cancer. On the other hand, the similarities between normal and malignant stem cells predict that such treatments may also possess significant toxicities. Recent encouraging data have provided proof of principle that selective targeting of CSCs is possible (Yilmaz et al., 2006). However, the development of anti-CSC therapies for each type of cancer is likely to require the identification of factors that maintain CSCs, but not normal stem cells, in each tissue.

One important difference between normal stem cells and CSCs might be the degree to which these cells are regulated by the immediate microenvironment. Stem cells of various tissues exist within protective niches that are composed of a number of differentiated cell types (Fuchs et al., 2004; Moore and Lemischka, 2006). These mature cells provide direct cell contacts and secreted factors that maintain stem cells primarily in a quiescent state. For example, histologic and ex vivo cell culture studies of mouse tissues suggest that neural stem cells lie within a vascular niche in which endothelial cells regulate stem cell self-renewal (Louissaint et al., 2002; Palmer et al., 2000; Ramirez-Castillejo et al., 2006; Shen et al., 2004). Thus, CSCs might arise from normal stem cells that have acquired mutations that enable them to escape

SIGNIFICANCE

We present evidence that brain tumors orchestrate vascular niches that maintain the CSC pool. Disruption of these niche microenvironments ablates the fraction of self-renewing cells in brain tumors and arrests tumor growth. Our data identify a potential role for niche microenvironments in the maintenance of brain CSCs and identify a mechanism by which antiangiogenic drugs inhibit brain tumor growth.

from niche control (Wodarz and Gonzalez, 2006). Alternatively, deregulation of extrinsic factors within the niche might lead to uncontrolled proliferation of stem cells and tumorigenesis (Clarke and Fuller, 2006). If CSCs depend upon aberrant niche microenvironments, then these niches might represent targets for treatments of cancer.

Here, we demonstrate that Nestin$^+$/CD133$^+$ cancer cells that include the CSC fraction are located next to capillaries in brain tumors. We show further that endothelial cells interact selectively with Nestin$^+$/CD133$^+$ brain cancer cells in culture and supply secreted factors that maintain these cells in a self-renewing and undifferentiated state. Increasing the number of endothelial cells or blood vessels in orthotopic brain tumor xenografts expanded the numbers of self-renewing Nestin$^+$/CD133$^+$ cancer cells and accelerated the initiation and growth of tumors. Conversely, antiangiogenic therapies depleted tumor blood vessels and associated self-renewing Nestin$^+$/CD133$^+$ cancer cells from xenografts and arrested tumor growth. Thus, we propose that the brain tumor microvasculature forms niche microenvironments that maintain CSCs and that represent therapeutic targets in brain tumors.

RESULTS

Nestin$^+$ Brain Tumor Cells Associate with the Tumor Vasculature

Normal neural stem and precursor cells and brain CSCs express the major intermediate filament protein Nestin (Galli et al., 2004; Hemmati et al., 2003; Palmer et al., 2000; Singh et al., 2004; Taylor et al., 2005). In the hippocampus, Nestin$^+$ cells are located close to capillaries where endothelial cells are believed to regulate the self-renewal and differentiation of stem cell daughters (Palmer et al., 2000; Wurmser et al., 2004). As a first step to establish if brain CSCs are located within a vascular niche, we determined the incidence of Nestin$^+$ cells, and the proximity of these cells to tumor capillaries in sections of medulloblastoma (n = 20), ependymoma (n = 23), oligodendroglioma (n = 20), and glioblastoma (n = 10).

In keeping with the low incidence of CSCs within brain tumors (Galli et al., 2004; Singh et al., 2004; Taylor et al., 2005), between 0.15% and 0.22% of cells within tumors were Nestin$^+$ (>500 cells counted per tumor section; Figure 1A). The number of Nestin$^+$ cells in brain tumors appeared to correlate with microvessel density (MVD): oligodendrogliomas and glioblastomas that had the highest MVD also contained the greatest numbers of Nestin$^+$ cells (Figure 1A). Further, Nestin$^+$ cells were located significantly closer to tumor capillaries than Nestin$^-$ cells, independent of histologic diagnosis (Figures 1A and 1B).

Since individual tumor sections represent three dimensional tissues in only two dimensions, it is difficult using standard histology to determine the precise relationship between individual cells and the vasculature (Palmer et al., 2000). Therefore, we used multiphoton laser-scanning microscopy to reconstruct, in three dimensions, serial images taken through 50 μm sections of four gliomas that were coimmunostained for CD34 and Nestin (~70 images per section). This analysis showed clearly that Nestin$^+$ tumor cells directly contact tumor capillaries (Figure 1C).

Endothelial cells have been reported to express Nestin (Aihara et al., 2004). However, the morphology of Nestin$^+$ cells in brain tumors was more typical of neural stem cells, and less than 0.1% of these cells coexpressed the endothelial marker CD34. Furthermore, 73.4% ± 20% of Nestin$^+$ cells in tumor sections coexpressed the cell surface protein CD133, which marks quite specifically normal neural stem and precursor cells and brain CSCs (>800 cells counted per tumor; Figure 1D) (Singh et al., 2004; Taylor et al., 2005; Uchida et al., 2000).

Focusing on medulloblastoma, we next sought to determine if Nestin$^+$ cells in brain tumors are cancer cells or entrapped normal neural stem and precursor cells. First, we performed consecutive coimmunofluorescence (Nestin and CD34) and fluorescence in situ hybridization (FISH) analysis of sections of medulloblastomas that we had shown previously to contain an isochromosome of 17q (Thompson et al., 2006). Over one-third of the Nestin$^+$-vessel-associated cells in these tumors contained an isochromosome 17q, confirming that they are cancer cells (Figure 1D). It is likely that a greater proportion of Nestin$^+$ cells in these tumors are cancer cells, since FISH underestimates the frequency of low-copy-number cytogenetic alterations because portions of cell nuclei are lost during tissue sectioning. Indeed, Ki-67/Nestin coimmunofluorescence demonstrated that 29.1% ± 11.6% of Nestin$^+$ cells in these tumors are proliferating (>500 cells counted per section; Figure 1D). Less than 1% of cells in the normal human subventricular zone express Ki-67 (Quinones-Hinojosa et al., 2006; Sanai et al., 2004). Therefore, Nestin$^+$ cells in medulloblastoma appear to possess aberrant proliferative capacity, suggesting further that they are cancer cells.

Finally, we prelabeled Daoy (Jacobsen et al., 1985) and MEB-MED-8A (Pietsch et al., 1994) medulloblastoma cells with green fluorescence protein (GFP) by retroviral transduction and transplanted 1 × 10^6 GFP$^+$ cells orthotopically into the brains of immunocompromised mice (n = 3 mice per cell line). Engrafted Daoy and MEB-MED-8A cells formed highly infiltrative primitive neuroectodermal tumors (Figure 1E and data not shown). CSCs have been identified in established brain tumor cell lines and are responsible for the in vivo malignancy of these cells (Kondo et al., 2004). In keeping with our analysis of primary medulloblastomas, 0.83% and 1.3% of cells in Daoy and MEB-MED-8A xenografts, respectively, expressed Nestin (>300 cells counted per tumor; Figure 1E), and these cells were located significantly closer to capillaries (Daoy, 32 ± 3.3 μm; MEB-MED-8A, 44 ± 5.6 μm) than were Nestin$^-$ cells (Daoy, 74 ± 2.5 μm; MEB-MED-8A, 80 ± 3.6 μm; $p < 0.0001$ for both cell lines). Nestin$^+$ cells in these xenografts coexpressed GFP, confirming that they are cancer cells (Figure 1E). Together, these data indicate that the great majority of Nestin$^+$ cells in brain tumors are vessel-associated cancer cells.

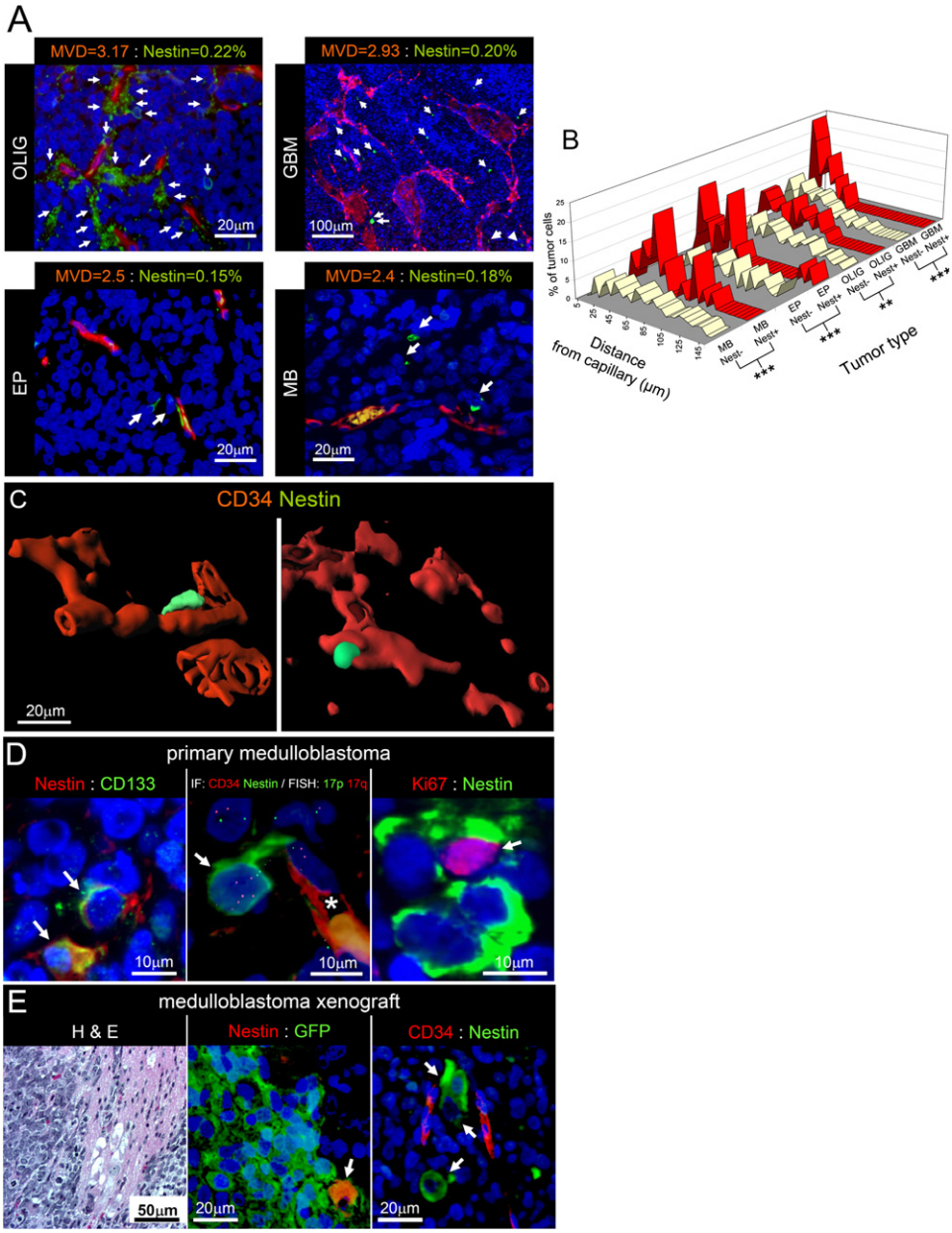

Figure 1. Nestin$^+$ Cells in Brain Tumors Are Located Next to Capillaries

(A) Coimmunofluorescence analysis of Nestin and CD34 expression in sections of a primary medulloblastoma (MB), ependymoma (EP), oligodendroglioma (OLIG), and glioblastoma (GBM). Arrows indicate Nestin$^+$ cells. The microvessel density (MVD) and percentage Nestin$^+$ tumor cells are shown for each tumor type.

(B) Graph reports the percentage of Nestin$^+$ and Nestin$^-$ cells that were located in incremental distances of 5 μm from the nearest CD34$^+$ endothelial cell in each tumor type (**$p < 0.005$, ***$p < 0.0005$ for the average distance of Nestin$^+$ versus Nestin$^-$ cells from CD34$^+$ cells).

(C) Reconstruction in three dimensions of capillaries (CD34, red) and Nestin$^+$ tumor cells (green) in 50 μm sections of two gliomas.

(D) Nestin and CD133 coimmunofluorescence (left), concurrent coimmunofluorescence (Nestin/CD34) and FISH (17p/17q) (middle), and coimmunofluorescence (Nestin/Ki-67) staining (right) of primary medulloblastoma. Asterisks marks a capillary lumen.

(E) Hematoxylin and eosin staining (left), Nestin and GFP coimmunofluorescence (middle), and Nestin and CD34 coimmunofluorescence (right) of orthotopic xenografts of GFP$^+$ Daoy medulloblastoma cells. Arrows indicate Nestin$^+$ cancer cells. All nuclei are stained with DAPI.

CD133$^+$ Brain Tumor Cells Interact Physically with Endothelial Cells in Culture

To investigate further if brain CSCs interact directly with endothelial cells, we prepared single-cell suspensions from a freshly resected primary medulloblastoma (MB5) and ependymoma (EP1) that we obtained direct from the operating room and labeled these with a green fluorescent dye (PKH67). We then used antibody-based cell sorting to

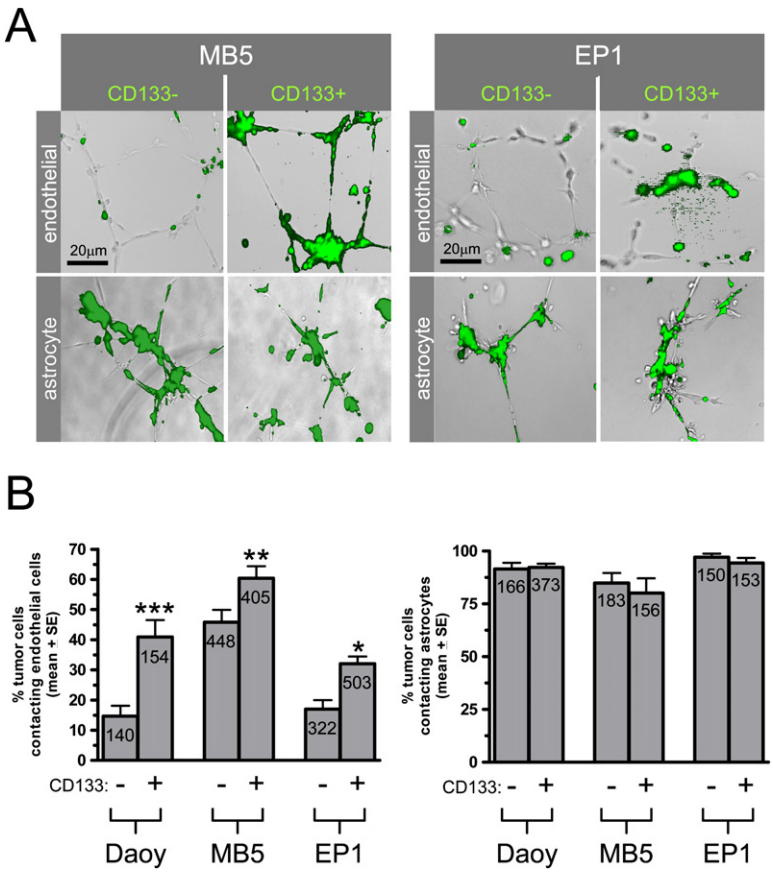

Figure 2. CD133$^+$ Brain Tumor Cells Associate with Endothelial Cells in 3D Matrigel Cultures

(A) Overlay of phase-contrast and autofluorescence photomicrographs of unlabeled endothelial cells or astrocytes that were cocultured with CD133$^+$ or CD133$^-$ green fluorescence-labeled primary medulloblastoma (MB5) or ependymoma (EP1) cells.

(B) The number of green fluorescent (tumor cells) that contacted directly an unlabeled cell (endothelial or astrocyte) was determined by high-power microscopic review of cocultures. The reviewer was blinded to CD133 tumor cell status. Graph reports the percentage of CD133$^+$ and CD133$^-$ tumor cells in each coculture that formed a direct contact with cocultured cells. Each bar is marked with the total number of tumor cells in each culture (*$p < 0.05$, **$p < 0.005$, ***$p < 0.0005$ reports the difference between CD133$^+$ and CD133$^-$ tumor cell contacts with cocultured cells).

isolate CD133$^+$ cells from these brain tumors since this fraction is enriched for CSCs (Singh et al., 2004; Taylor et al., 2005). Subsequent karyotype analysis of these tumor cells that we have reported elsewhere confirmed that they are cancer cells (Taylor et al., 2005). We similarly fractionated populations of Daoy medulloblastoma cells. We then mixed CD133$^+$ or CD133$^-$ tumor cells with primary human endothelial cells (PHECs) in a 3D matrigel assay in which the endothelial cells form vascular tubes (n = 8 separate cultures per cell population).

PHECs formed vascular tubes within 5–7 hr independent of the CD133 status of the cocultured tumor cells (Figure 2A). CD133$^+$ tumor cells, independent of origin, associated rapidly with endothelial vascular tubes, forming intimate contacts often along the entire length of an endothelial tube (Figures 2A and 2B). In contrast, significantly fewer CD133$^-$ tumor cells made contacts with endothelial cells and generally remained rounded and separate from the vascular-like structures. To control for the possibility that CD133$^-$ tumor cells are unable to form cell-cell contacts in 3D matrigel cultures, we repeated these experiments using primary human astrocytes (PHAs) instead of PHECs. Both CD133$^+$ and CD133$^-$ tumor cells interacted readily, but not differently, with PHAs in these cocultures (Figures 2A and 2B). Thus, CD133$^+$ brain tumor cells that contain the CSC fraction, but not CD133$^-$ cells, interact closely with vascular endothelial cells in culture.

Endothelial Cells Maintain Self-Renewing and Undifferentiated Brain Tumor Cells

Endothelial cells secrete soluble factors that maintain the self-renewal and undifferentiated phenotype of normal neural stem cells (Ramirez-Castillejo et al., 2006; Shen et al., 2004). To test if endothelial-derived factors similarly maintain self-renewing brain tumor cells, we first passaged tumor spheres of CD133$^+$ cells that we isolated from a primary medulloblastoma (MB1), a primary ependymoma (EP1), and the Daoy medulloblastoma cell line, under conditions that promote stem cell growth (Taylor et al., 2005). Tumor spheres derived from each of these cell populations could be passaged serially and expressed CD133 and Nestin, confirming that these are clonogenic, self-renewing stem-like cells (Figures 3A–3C). We then transferred tertiary tumor spheres of these cells to the base of culture wells while the upper transwell compartment was seeded with PHECs or control cells (CD133$^-$ tumor cells, fibroblasts, or PHAs) (Figure 3D). This transwell system allows the exchange of diffusible factors, but not cells, between chambers. Cocultures were maintained for 2 weeks in reduced-serum-containing medium.

Tumor spheres that were cocultured with PHECs increased in size and after 2 weeks were up to five times larger than those grown in the presence of control cells (Figure 3E). Further, significantly more PHEC-cocultured tumor spheres remained as intact CD133$^+$/Nestin$^+$ tumor

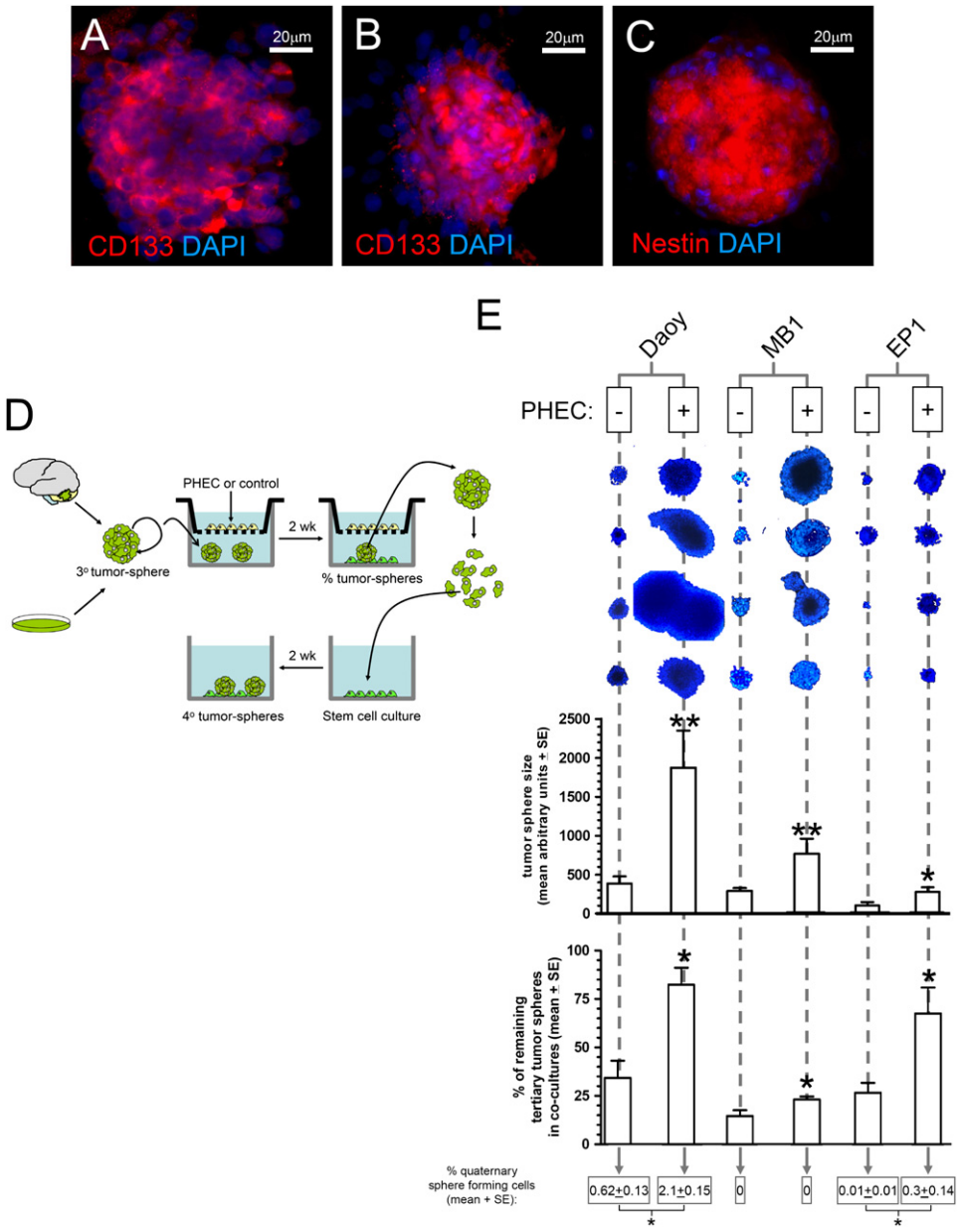

Figure 3. Endothelial Cells Maintain Self-Renewing and Undifferentiated Brain Tumor Cells in Culture

(A–C) CD133 and Nestin immunofluorescence analysis of Daoy (A)-, primary medulloblastoma (MB1) (B)-, and primary ependymoma (EP1) (C)-derived tertiary tumor spheres.

(D) Cartoon depicting the experimental approach adopted to determine the ability of PHECs to maintain the self-renewal and undifferentiated phenotype of brain tumor cells.

(E) Comparison of the size (top images: DAPI staining of four representative tumor spheres; top graph: average total sphere area of tumor spheres in the appropriate cultures), maintenance (bottom graph: percentage of tertiary tumor spheres remaining after 120 hr of coculture), and self-renewal (bottom figures report the percentage of quaternary-forming tumor spheres derived from cocultured tertiary spheres) of Daoy medulloblastoma cells and primary medulloblastoma (MB1) and primary ependymoma (EP1) cells cocultured with PHECs (+) or control cells (–). Results are shown for differentiated tumor cells as controls. Similar results were obtained when PHAs or fibroblasts were used as controls (*$p < 0.05$, **$p < 0.005$, exact Wilcoxon test).

spheres compared to those cultured with control cells. Thus, PHECs maintained the proliferation of tumor sphere cells even under reduced-serum conditions that caused control cultured spheres to disaggregate, spread out over the culture surface, and lose expression of CD133 and Nestin (Figure 3E and data not shown).

To test if PHECs maintained also the self-renewal capacity of brain tumor cells, we disaggregated tertiary

tumor spheres that had been cocultured for 2 weeks with either PHECs or control cells and reseeded suspensions of these cells in stem cell culture medium that was serum free (Figure 3D). Although we were unable to recover any quaternary tumor spheres from cultures of MB1 cells, both Daoy- and EP1-derived sphere cells that had been cocultured with PHECs were significantly more likely to generate quaternary tumor spheres than cells isolated from control cocultures (Figure 3E). These data identify striking similarities between normal neural stem cells and self-renewing brain tumor cells and suggest that stem-like properties of brain CSCs are enhanced by endothelial-cell-secreted factors.

Endothelial Cells Promote the Propagation of Brain Tumors In Vivo

If endothelial-derived factors support the self-renewal of brain CSCs, then we reasoned that endothelial cells should promote the propagation of brain tumors in vivo. To test this, we injected 1×10^6 unsorted GFP^+ Daoy medulloblastoma cells either alone or in combination with red fluorescence dye (PKH26)-labeled PHECs, under cranial windows in the cerebral cortex of immunocompromised mice ($n \geq 3$ mice per cell mix). Tumor cells (green) were readily distinguished from endothelial cells (red) using dual-color fluorescence microscopy (Figure 4A).

Injections of GFP^+ Daoy cells alone resulted in a steady increase in tumor fluorescence (green) that could be detected using intravital fluorescence microscopy via the cranial window, and that correlated closely with increasing tumor burden (Figure 4A and Figure S1 in the Supplemental Data available with this article online). Tumor fluorescence reached a peak in these mice at around 7 weeks postinjection, at which point the animals succumbed to their disease (mean peak fluorescence at 7 weeks; 526 ± 176 SD; n = 6 independent animals; see Figure S1). Remarkably, 1×10^6 GFP^+ Daoy medulloblastoma cells that were coinjected with 100,000 PHECs formed tumors much more rapidly, reaching peak tumor burden after only 4 weeks (Figure 4A). This acceleration of xenograft growth occurred in a cell-dose- and cell-specific manner: increasing numbers of coinjected PHECs produced a stepwise increase in tumor growth rate, but coinjection of PHAs did not affect xenograft growth (Figure 4A). Red fluorescence declined steadily in PHEC/tumor cell xenografts, since the half-life of PKH26 dye in vivo is ~2 weeks. Thus, the increasing tumor fluorescence in these xenografts resulted entirely from the expansion of the tumor cell population.

Xenografts that were established in the presence of PHECs contained up to 25 times more $Nestin^+/GFP^+$ tumor cells than did xenografts of Daoy cells alone (cells detected by Nestin/GFP coimmunofluorescence; Figure 4B). PHECs (differentiated from endogenous mouse endothelial cells using a human CD34-specific antibody; Figure S2) coclustered with $Nestin^+/GFP^+$ tumor cells in xenografts (Figure 4C). Importantly, PHECs remained separate from tumor capillaries and did not increase the MVD of xenografts relative to that observed in tumors formed by GFP^+ Daoy cells alone (data not shown). Together, these data suggest the hypothesis that endothelial cells contribute specific factors to the tumor microenvironment that expand the CSC pool and accelerate the initiation and/or growth of brain tumor xenografts.

To test more directly if endothelial cells promote tumor growth by supporting CSCs, and if freshly resected primary tumor cells are responsive to these signals, we repeated our cranial window transplant experiments using 50,000 $CD133^+$ or $CD133^-$ cells that we isolated from two primary medulloblastomas (MB4 and MB5). Primary tumor cells were obtained direct from the operating room, GFP-labeled by lentiviral transduction, and then transplanted as described below after less than four passages in culture. Two out of every three primary medulloblastomas can be expected to generate tumors following orthotopic transplant of 50,000 $CD133^+$ tumor cells, but no significant tumor growth has been reported from injections of $CD133^-$ tumor cells (Singh et al., 2004). As expected, $CD133^-$ primary tumor cells grew only transiently (MB4) or not at all (MB5) as transplants, even in the presence of coinjected PHECs (Figure 5). In contrast, $CD133^+$ tumor cells formed fluorescent masses within 7 days of injection. The growth of $CD133^+$ cell masses was enhanced dramatically by the presence of PHECs and resulted in the formation of a rapidly growing tumor in mice that were injected with $CD133^+$ MB5 cells. While coinjection of PHECs also enhanced initially the growth of transplanted $CD133^+$ MB4 cells, the growth of these tumor cells was not sustained. Together, these data support the hypothesis that endothelial cells contribute to a niche microenvironment that promotes the initiation of brain tumors by CSCs.

Depletion of Brain Tumor Blood Vessels Eradicates Self-Renewing Tumor Cells

Our finding that endothelial-derived factors enhance the initiation of brain tumors by $CD133^+$ tumor cells suggests that antiangiogenic drugs could inhibit brain tumor growth, at least in part, by disrupting a CSC vascular niche. To test this, we investigated the impact of antiangiogenic therapies on the numbers of self-renewing tumor cells in, and growth of, medulloblastoma and glioma orthotopic xenografts.

Angiogenic signaling in tumors is often initiated by oncogenic cell signal pathways (Jain et al., 2006). Therefore, we first upregulated angiogenic signaling in GFP^+ Daoy cells by transfection with the *ERBB2* oncogene ($Daoy^{ERBB2}$). ERBB2 is overexpressed in aggressive forms of medulloblastoma (Gajjar et al., 2004) and elicits a cell signal that upregulates vascular endothelial growth factor (VEGF) (Saucier et al., 2004). $Daoy^{ERBB2}$ cells secreted 60-fold more VEGF than did vector control ($Daoy^V$) cells, and treatment of these cells with Erlotinib—a selective inhibitor of the EGFR and ERBB2 tyrosine kinases (Akita and Sliwkowski, 2003)—or an anti-ERBB2 siRNA downregulated VEGF expression (see Figures S3A and S3B). We then established orthotopic xenografts of 1×10^6 GFP^+ $Daoy^{ERBB2}$ or $Daoy^V$ cells under cranial windows in the

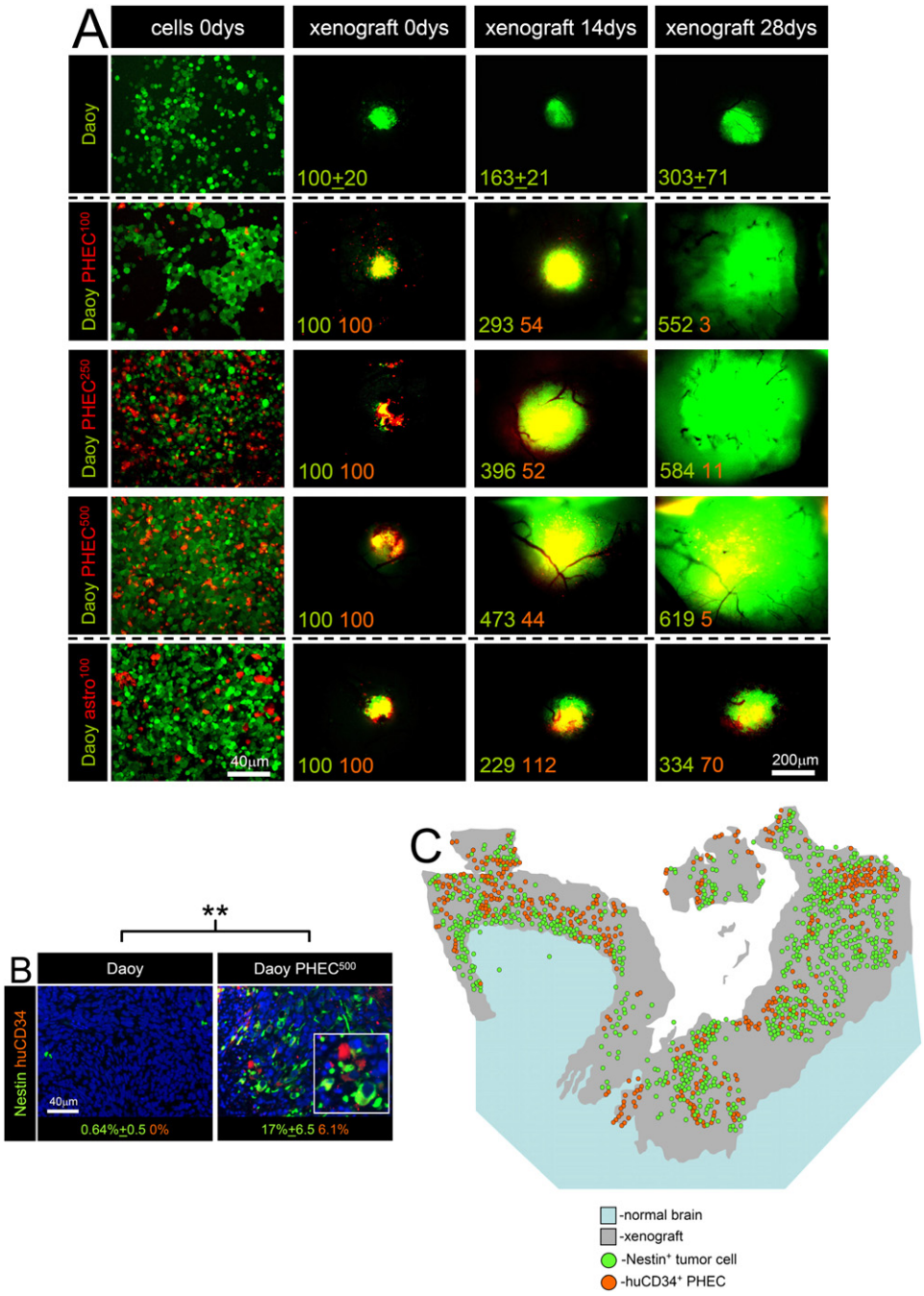

Figure 4. Endothelial Cells Promote the Growth of Orthotopic Brain Tumor Xenografts

(A) The first column shows autofluorescence micrographs of mixed suspensions of GFP$^+$ Daoy cells (green) and PHECs or PHAs (red) just prior to orthotopic injection. Numbers of PHECs and PHAs are in thousands. Subsequent columns show overlaid intravital red and green fluorescence photomicrographs of xenografts that were captured via the cranial window at the indicated time intervals following transplantation. Numbers report the level of green and red fluorescence in each xenograft at each time point (percentage of day 0 value).

(B) Coimmunofluorescence (Nestin and human-specific CD34) analysis of the orthotopic xenografts in (A) that were established by transplantation of Daoy cells alone (left) or Daoy cells plus 500 × 10^3 PHECs (right). Numbers at the bottom of each photomicrograph report the percentage of Nestin (green) and human CD34 (red)-expressing cells in each tumor (**$p < 0.005$, exact Wilcoxon test).

(C) Map of the distribution of Nestin and human CD34-expressing cells across an entire section of a Daoy orthotopic xenograft that included 500 × 10^3 PHECs. The map was generated from a composite review of high-power coimmunofluorescence photomicrographs.

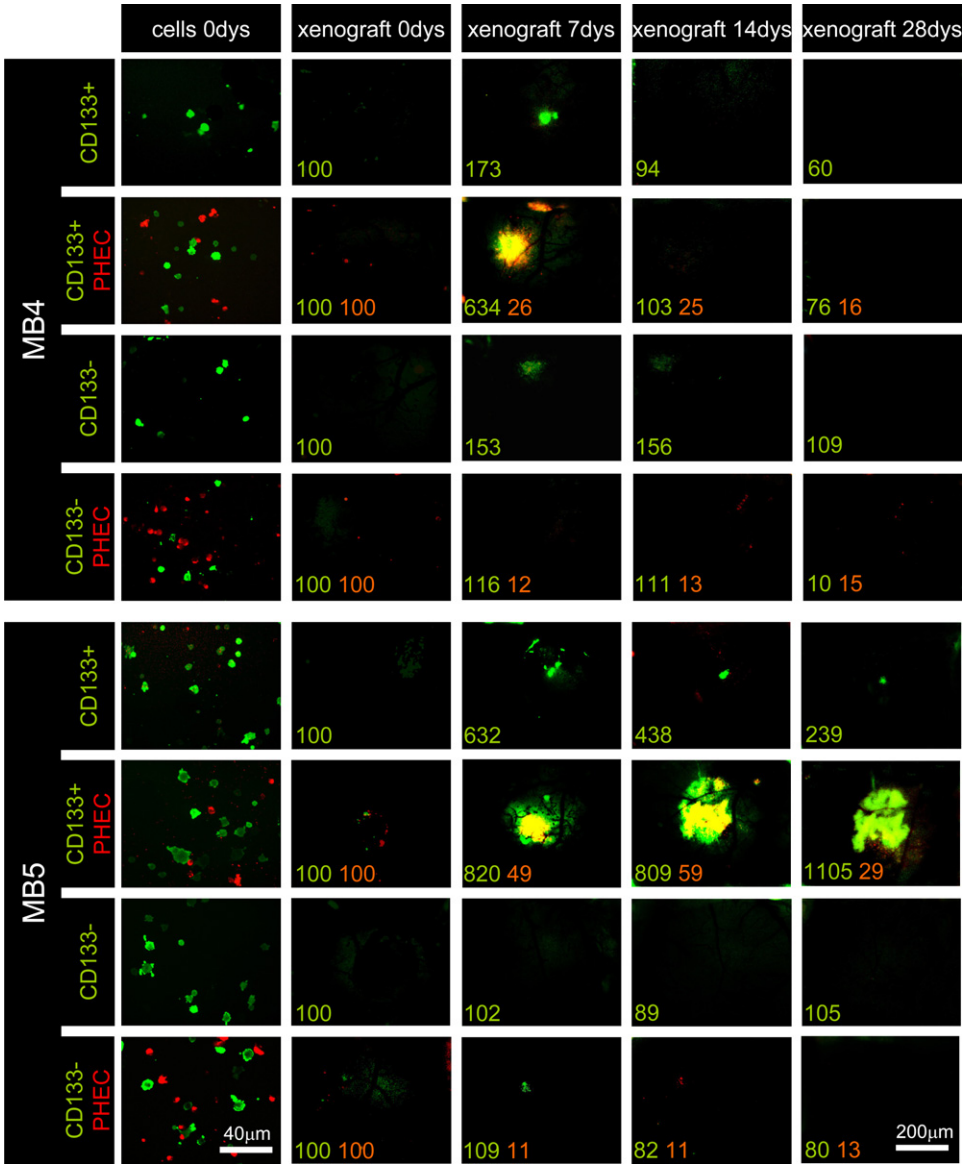

Figure 5. Endothelial Cells Promote the Initiation of Orthotopic Brain Tumor Xenografts by CD133$^+$, but Not CD133$^-$ Primary Medulloblastoma Cells

Autofluorescence photomicrographs of the growth of orthotopic xenografts of 50,000 GFP-labeled CD133$^+$ or CD133$^-$ cells that we isolated from two primary medulloblastomas (MB4 and MB5) and transplanted orthotopically under cranial windows into the cerebral cortex of nude mice. Tumor cells were transplanted alone or with 50,000 red fluorescence-labeled PHECs. The first column shows autofluorescence micrographs of cells immediately prior to transplantation. Subsequent columns show overlaid intravital red and green fluorescence microscopy images of tumors captured via the cranial window at the indicated time intervals following implantation. Numbers report the level of green and red fluorescence in each xenograft at each time point (percentage of day 0 value).

cerebral cortex of nude mice. To target both the "upstream" and "downstream" components of angiogenic signaling in this model, we treated tumor-bearing mice with either Erlotinib (50 mg/kg/2× day for 5 days), which abolishes ERBB2 signaling in vivo (Hernan et al., 2003); a single dose of 10 mg/kg of the anti-VEGF monoclonal antibody Bevacizumab; or vehicle-only control (n = 10 mice bearing each xenograft for each treatment). Tumors were then excised and analyzed as outlined in Figure 6A.

As expected, Daoy^{ERBB2} xenografts expressed much higher levels of VEGF, contained a significantly higher MVD (compare vehicle-only treated tumors in Figures 6B and 6C), and grew more rapidly following transplantation (Figure S4) than did Daoy^V tumors. Also, single-cell suspensions of excised Daoy^{ERBB2} tumors generated five times more self-renewing CD133$^+$/Nestin$^+$ tumor spheres than cells from Daoy^V tumors (compare vehicle-only treated tumors in Figure 6D). All tumor sphere cells

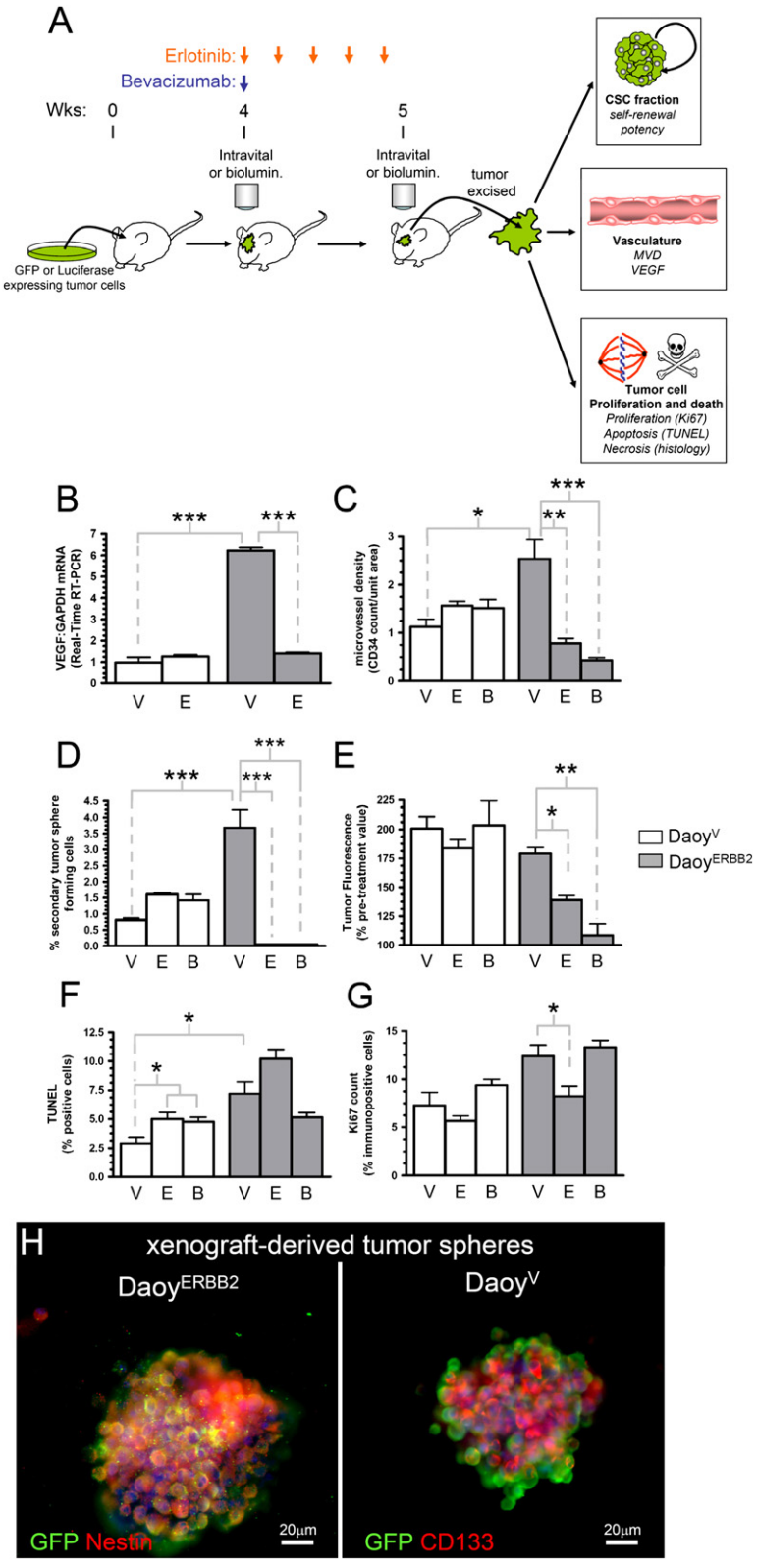

Figure 6. Antiangiogenic Therapy Depletes the Tumor Vasculature, Ablates Self-Renewing Tumor Cells, and Inhibits the Growth of Daoy^{ERBB2} Orthotopic Xenografts

(A) Cartoon depicting the experimental approach adopted to determine whether depletion of blood vessels from brain tumors ablates the CSC fraction.

(B–G) Graphs (all error bars = mean ± SE) report VEGF expression levels (B), microvessel density (C), self-renewal capacity (serial tumor sphere-forming assay) (D), growth (tumor fluorescence) (E), apoptosis (TUNEL) (F), and proliferation (Ki67 labeling) (G) of vehicle ("V")-, Erlotinib ("E")-, or Bevacizumab ("B")-treated Daoy^{ERBB2} and Daoy^{V} orthotopic xenografts (*$p < 0.05$, **$p < 0.005$, ***$p < 0.0005$, exact Wilcoxon test).

(H) Coimmunofluorescence analysis of tumor spheres formed ex vivo by cells that were derived from vehicle-treated Daoy^{ERBB2} and Daoy^{V} xenografts.

coexpressed GFP, confirming that they were derived from transplanted tumor cells and not normal mouse cells (Figure 6H), and displayed evidence of multipotency when cultured under conditions that promote differentiation (Figure S5). Importantly, ERBB2 signaling in Daoy cells does not impact directly cell proliferation, apoptosis,

or self-renewal (see Figures S6A to S6D). Thus, expansion of the tumor vasculature in Daoy^{ERBB2} relative to Daoy^{V} tumors was associated with an increased number of self-renewing, multipotent cancer cells.

Both Erlotinib and Bevacizumab treatments induced a profound antiangiogenic response in Daoy^{ERBB2} xenografts that was associated with significant tumor growth arrest (Figures 6B, 6C, and 6E). Interestingly, despite these marked antiangiogenic and growth inhibitory effects, neither drug altered the level of apoptosis or necrosis in Daoy^{ERBB2} xenografts, and only Erlotinib decreased slightly cell proliferation in these tumors relative to vehicle treatment (Figures 6F and 6G and data not shown). However, both drugs resulted in a complete loss of self-renewing GFP^{+}/Nestin^{+}/CD133^{+} tumor cells from single-cell suspensions of treated Daoy^{ERBB2} xenografts (Figure 6D). In stark contrast, since the ERBB2-VEGF axis in Daoy^{V} tumors is much less active than in Daoy^{ERBB2} xenografts, neither Erlotinib nor Bevacizumab affected the MVD in Daoy^{V} tumors (Figure 6C). In agreement with our hypothesis, these treatments also failed to alter the number of self-renewing GFP^{+}/Nestin^{+}/CD133^{+} cells in Daoy^{V} tumors (Figure 6D). Although both Erlotinib and Bevacizumab therapy produced a moderate increase in Daoy^{V} tumor cell apoptosis that presumably resulted from blockade of endogenous EGFR/ERBB2 and VEGF signaling, this did not impact tumor growth (Figures 6E and 6F). Importantly, neither Erlotinib nor Bevacizumab affect directly the self-renewal, proliferation, or apoptosis of Daoy cells in culture (see Figure S6E and data not shown). Together, these data provide strong support for the hypothesis that brain tumor growth depends critically upon the presence of an intact CSC vascular niche and identifies this niche as a potential target for treatments of brain tumors. As a first step to determine if this therapeutic approach might have clinical benefit, we treated Daoy^{ERBB2} and Daoy^{V} tumor-bearing mice for 2 weeks with 50 mg/kg/2× day of Erlotinib (n = 8 mice with each tumor per treatment). Erlotinib prolonged significantly the survival of mice bearing Daoy^{ERBB2} tumors (median survival of Erlotinib-treated mice = 66 ± 3.4 days versus 45 ± 2.9 days in vehicle-treated mice; exact log rank $p < 0.05$), but not those harboring Daoy^{V} xenografts (median survival of Erlotinib-treated mice = 53 ± 2.8 days versus 54 ± 3.1 days in vehicle-treated mice; log rank $p = 0.73$).

Finally, since ongoing clinical trials of Bevacizumab suggest that this drug has promising therapeutic activity against glioblastoma (Reardon and Wen, 2006), we investigated if Bevacizumab might deplete self-renewing cancer cells from this brain tumor. To do this, we treated with Bevacizumab or vehicle mice bearing orthotopic xenografts of U87 glioma cells that express the Luciferase reporter gene (U87G^{Luc}). Transplantation of 1×10^{6} U87^{Luc} cells into the brains of immunocompromised mice resulted in the formation of brain tumors that could be detected readily using bioluminescence (Figure 7A). As we observed in Daoy^{ERBB2} medulloblastoma xenografts, a single dose of 10 mg/kg Bevacizumab, but not vehicle, reduced markedly the MVD and growth of U87^{Luc} tumors (n = 5 mice per treatment group; Figures 7A–7C). Furthermore, Bevacizumab decreased profoundly the numbers of vessel-associated Nestin^{+} tumor cells in U87^{Luc} xenografts and the number of self-renewing GFP^{+}/Nestin^{+}/CD133^{+} tumor cells that could be recovered from these tumors, without impacting tumor cell proliferation, apoptosis, or necrosis (Figures 7A and 7D–7G and data not shown). Interestingly, residual Nestin^{+} cells in Bevacizumab-treated glioma xenografts were not distributed randomly through tumors but were associated with persisting tumor vessels (Figure 7A). Thus, we propose that antiangiogenic drugs arrest brain tumor growth, at least in part, by disrupting a vascular niche microenvironment that is critical for the maintenance of CSCs.

DISCUSSION

Evidence suggests that normal neural stem cells exist in vascular niches, into which endothelial cells secrete factors that regulate neural stem cell function (Palmer et al., 2000; Ramirez-Castillejo et al., 2006; Shen et al., 2004). Here, we provide several lines of evidence that the brain tumor microvasculature forms a niche that is critical for the maintenance of CSCs.

Since niches control stem cell function, it may seem counterintuitive that CSCs would be located within these regulatory microenvironments. However, our data support the hypothesis that vascular niches in brain tumors are abnormal and contribute directly to the generation of CSCs and tumor growth. In the normal brain, neural stem cell niches are restricted to the hippocampus and subventricular zones where rates of cell proliferation are quite low (Sanai et al., 2005). In contrast, we found that a significant proportion of vessel-associated Nestin^{+} tumor cells are proliferating, and that these cells are distributed throughout tumors, from all regions of the cerebrum and cerebellum. We show further that PHECs maintain self-renewing brain tumor cells in culture and promote the initiation and growth of orthotopic brain tumor xenografts. Increasing the number of capillaries in orthotopic brain tumors also expanded dramatically the number of self-renewing and multipotent cells contained in these tumors. Therefore, we propose that the tumor microvasculature generates specific niche microenvironments that promote the formation and/or maintenance of brain CSCs. Interestingly, atypical ectopic perivascular niches were recently described around perivascular areas of the inflamed CNS (Martino and Pluchino, 2006). These entities behave as anatomically atypical, although highly specialized, ectopic niches that regulate long-term survival and behavior of transplanted neural stem cells. Thus, atypical and ectopic stem cell niches might play central roles in a number of nervous system diseases, including brain tumors.

If the recruitment of aberrant vascular niches is an important component in the progression of brain tumors, then this might explain why the most aggressive brain tumors are highly angiogenic (Folkerth, 2004; Phillips et al., 2006; Plate et al., 1992). Intriguingly, protein ligands

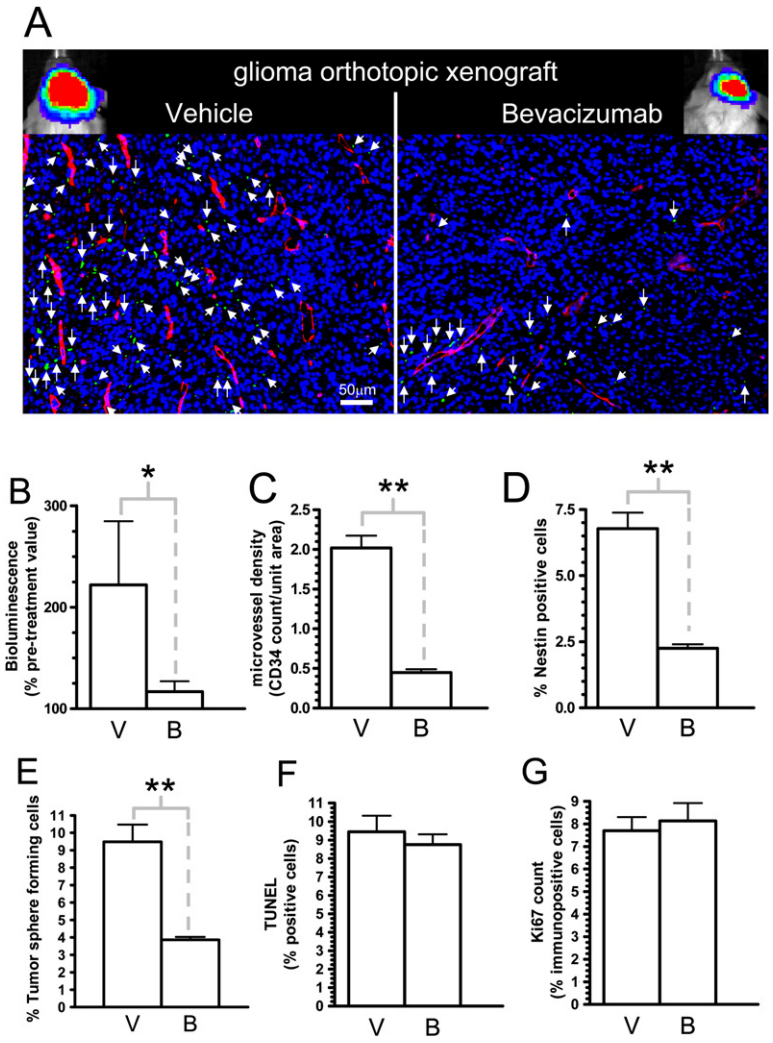

Figure 7. Bevacizumab Therapy Depletes the Tumor Vasculature, Ablates Self-Renewing Tumor Cells, and Inhibits the Growth of U87^{Luc} Glioma Orthotopic Xenografts

(A) Coimmunofluorescence analysis of Nestin and CD34 expression in sections of glioma xenografts 1 week following treatment with Bevacizumab or vehicle. Arrows point to Nestin$^+$ cells. Bioluminescence images of these tumors generated prior to excision are shown above.

(B–G) Graphs (all error bars = mean ± SE) report tumor growth (bioluminescence) (B), microvessel density (C), percentage Nestin$^+$ cells (D), self-renewal capacity (serial tumor sphere-forming assay) (E), apoptosis (TUNEL) (F), and proliferation (Ki67 labeling) (G) of vehicle ("V")- and Bevacizumab ("B")-treated xenografts (*$p < 0.05$, **$p < 0.005$, exact Wilcoxon test).

that are found within the neural stem cell niche have been shown to regulate both stem cell self-renewal and angiogenesis, suggesting further that these two processes are linked. For example, KIT ligand (also known as stem cell factor), which is a potent glioma-derived proangiogenic factor (Sun et al., 2006), also promotes the migration, survival, and proliferation of neural progenitor cells (Erlandsson et al., 2004; Jin et al., 2002), and PEDF, which maintains neural stem cell self-renewal, is a potent regulator of angiogenesis (Pumiglia and Temple, 2006; Ramirez-Castillejo et al., 2006). Furthermore, very recent studies of orthotopic glioblastoma xenografts suggest that CSCs of this brain tumor secrete angiogenic factors that promote the recruitment and formation of tumor blood vessels (Bao et al., 2006). It is noteworthy that VEGFR-1$^+$ bone marrow progenitor cells were shown recently to form niches at the sites of lung and melanoma tumor metastasis (Kaplan et al., 2005), and that bone marrow endothelial niches are required for the homing and retention of normal hematopoietic and leukemic stem cells (Kiel et al., 2005; Sipkins et al., 2005). In the brain, the formation of multiple vascular CSC niches, each with the capacity to generate numerous tumor cells, might facilitate significantly brain tumor growth and invasion.

As well as regulating stem cell proliferation and cell-fate decisions, niches also play a protective role, shielding stem cells from environmental insults. Thus, vascular niches might protect brain CSCs from chemo- and radiotherapies, enabling these cells to reform a tumor mass following an initial clinical response. Evidence indicates that endothelial cells can protect stem cells and tumor cells from radiation damage (Garcia-Barros et al., 2003; Paris et al., 2001). For example, solid tumor xenografts grown in mice with radiation-resistant endothelial cells are much less sensitive to radiation damage than tumors grown in wild-type mice (Garcia-Barros et al., 2003). Our data suggest a mechanism, at least in brain tumors, by which endothelial cells might promote tumor radioresistance. Further, studies of the hematopoietic stem cell niche suggest that niche microenvironments can promote cell survival signals in CSCs, enabling them to resist chemotherapies (De Toni et al., 2006; Dick and Lapidot, 2005).

If the notion that niches protect CSCs proves correct, then targeting these microenvironments could prove a highly effective treatment of cancer. We found that antiangiogenic therapies including Bevacizumab deplete tumor blood vessels and self-renewing cancer cells from orthotopic models of medulloblastoma and glioma, resulting in tumor growth arrest. Notably, VEGF has been shown to enhance the survival of neural stem cells (Wada et al., 2006). Thus VEGF-specific inhibitors like Bevacizumab might impact brain tumor growth by targeting both a vascular niche and the associated CSCs. Exciting early data from clinical trials of Bevacizumab combined with the chemotherapeutic drug CPT-11 suggest that this combination is one the most effective treatments of glioblastoma identified to date (Reardon and Wen, 2006). In light of our data, it is tempting to speculate that the activity of this drug combination results from targeting CSCs, as well as the disease bulk. This important mechanism of drug action should be studied further in ongoing preclinical and clinical trials of antiangiogenic drugs in brain tumors.

EXPERIMENTAL PROCEDURES

Tumor Samples and Cell Lines

Tumor samples were obtained under protocol XPD01-092 (St. Jude Children's Research Hospital Institutional Review Board). Tumors were immediately disaggregated into single-cell suspensions as described in detail elsewhere (Taylor et al., 2005). Primary tumor cell cultures were maintained in Neurobasal medium (Invitrogen) containing 2 mM L-glutamine, N2 supplement (Invitrogen), B27 supplement (Invitrogen), 20 ng/ml hrEGF (Invitrogen), 20 ng/ml hrbFGF (Invitrogen), and 50 μg/ml BSA. All experiments were conducted at cell passage <4. Previous cytogenetic studies showed that all cultured primary tumor cells were cancer cells (Taylor et al., 2005). PHECs, U87, and Daoy cells were obtained from the ATCC (Manassas, VA). PHAs were from Cambrex, MD. PHECs were cultured in endothelial cell growth medium (EGM) containing 2% fetal bovine serum (GIBCO, USA). PHAs were cultured in astrocyte growth medium that contains 2% serum (AGM, Cambrex). Daoy cells were transfected with the complete coding region of *ERBB2* ($Daoy^{ERBB2}$) or vector control ($Daoy^{V}$), and U87 glioma cells with the luciferase reporter, as described (Hernan et al., 2003). GFP was expressed in $Daoy^{V}$ and $Daoy^{ERBB2}$ by transduction with MSCV-IRES-GFP retrovirus. Primary tumor cells were labeled green by GFP-lentiviral transduction. GFP^{+} tumor cells were isolated by fluorescence-activated cell sorting (FACS). Daoy and U87 cells were maintained under standard culture conditions in DMEM containing 10% FCS unless otherwise specified.

Tumor Sphere Initiation Assays

Single-cell suspensions were made in Neurobasal medium in 96-well plates (diluted as 10,000 to 1 cells/well). The number of tumor spheres that formed subsequently per well was quantified after 14 days. Tumor spheres were then disaggregated and reseeded to evaluate self-renewal by formation of secondary tumor spheres. Where indicated, this process was repeated to form tertiary and quaternary tumor spheres.

Coculture Studies

For transwell coculture studies, tumor spheres were added in 500 μl of culture medium to each well of a 24-well coculture plate (BD Biosciences). Transwell inserts containing 0.4 μm diameter membrane pores that allow the passage of diffusible molecules, but not cells, were then placed into each well and seeded with 1×10^4 PHECs or control cells (see text). Plates were then incubated under standard culture conditions in medium containing 2% fetal calf serum for 120 hr, and the number of remaining tumor spheres was counted using phase-contrast microscopy. The self-renewal of tumor sphere cells cocultured with PHECs or control cells was determined using the tumor sphere initiation assay described above. The differentiation of tumor sphere cells in cocultures was determined by seeding tumor spheres in culture wells on coated coverslips (poly-D-lysine/laminin) (BD Biosciences); tumor cells were then fixed with 4% paraformaldehyde and analyzed by immunofluorescence using previously published antibodies and techniques (Taylor et al., 2005). Neurosphere size was measured by analyzing ×200 magnification images of DAPI-stained tumor spheres and the ImageJ analysis tool (http://rsb.info.nih.gov/ij/).

For Matrigel coculture studies, GFP^{+} $Daoy^{V}$ or $Daoy^{ERBB2}$ cells or primary tumor cells prelabeled with PKH67 (Sigma) were sorted using CD133-antibody-coated magnetic beads (100 μl/10^8 cells; Miltenyi Biotec) as described (Taylor et al., 2005). Purity of CD133 populations was confirmed by CD133 immunofluorescence. Sorted tumor cells (6000 cells/ml) were cultured ± PHECs or PHAs (10,000 cells/ml) in Matrigel-coated (35 μl; BD BioScience) 8-well culture slides (BD BioScience) overnight at 37°C. PHECs or PHAs were imaged by phase-contrast microscopy, and sorted cells expressing GFP or stained with PKH67 were imaged using fluorescence microscopy.

Generation and Treatment of Orthotopic Transplants

Female CD-1 nu/nu mice (Charles River) aged 6–8 weeks were anesthetized and placed into stereotactic apparatus equipped with a Z axis (Kopf instruments). A small portion of the scalp was removed, a window (approximately 10 mm × 5 mm) was made in the skull using a dental drill, and the pial layer was removed. Tumor cells (1×10^6 in 5 μl Matrigel) were implanted with or without PHAs or PHECs into the cerebral surface at a depth of 0.5–2 mm using a 25 μl Hamilton syringe with an unbeveled 30G needle. The wound was then covered with a sterile glass window fixed in place using tissue adhesive. Immediately following wound closure, implanted animals were transferred to the intravital imaging system (Nikon, USA) and imaged to obtain a baseline measurement, and animals were reanesthetized as required for subsequent imaging. Data analysis was performed using MetaMorph Imaging software (Universal Imaging, Downington, PA). Measurements were restricted to a fixed region within each image throughout the course of the study and are presented as maximum fluorescence (F_{max}) normalized to minimum fluorescence (F_{min}), which compensated for potential interday variation in lamp intensity. $U87^{Luc}$ xenografts were prepared in a similar manner through small cranial burr holes without cranial windows. Tumor burden was measured in $U87^{Luc}$ tumor-bearing mice by bioluminescence using a Series IVIS Imaging System (Xenogen Corporation, Alameda, CA). Mice received an intraperitoneal injection of 15 mg/ml D-luciferin (Xenogen) in sterile PBS and were imaged 5 min later. All animals were imaged at a range of 25 cm for 10 s. Acquired images were analyzed with the use of Living Image Software version 2.50 (Xenogen). Bioluminescence measurements were recorded as photons per second.

Erlotinib (OSI Pharmaceuticals) was administered to tumor-bearing mice per os (p.o.) in a vehicle of 10% DMSO, 10% Cremephor in a 1% CMC solution. Animals were treated with Erlotinib (50 mg/kg/twice daily) or vehicle for 5 days. Treatment was repeated where indicated following a 2 day break. Bevacizumab (Genentech Inc.) was administered by tail-vein injection at a dose of 10 mg/kg. All animal procedures were conducted in accordance with all appropriate regulatory standards under protocol #356 (St. Jude Children's Research Hospital Animal Care and Use Committee).

Histologic, FISH, and Gene Expression Analysis

Dual-color FISH, immunofluorescence, immunohistochemical, and TUNEL analyses of formalin-fixed, paraffin-embedded tumor samples, xenografts, or cultured tumor cells were performed using immunoreagents, FISH probes, and methods as described previously (Taylor et al., 2005; Thompson et al., 2006). Nestin-specific antibodies

included a monoclonal antibody (Chemicon cat. no. MAB5326) that recognizes the human but not the mouse protein and a polyclonal antibody (Abcam) that recognizes human, mouse, and rat Nestin. The distance between Nestin$^+$ cells and CD34 endothelial cells was measured in dual-immunofluorescence-stained images of brain tumor sections using the line-measuring tool in ImageJ. In order to remove observer bias and to allow analysis of large numbers of tumor sections, immunohistochemical staining of xenografts, including assessment of MVD (CD34 staining), was scored blind to the xenograft and treatment using ImageJ software analysis. Briefly, images were processed at the same magnification (×200) by removal of background hematoxylin staining followed by monochromization. Monochrome images (giving binary data: black areas of immunohistochemical stain and white non-staining areas) were analyzed using ImageJ software, which calculated the absolute values for each channel, resulting in determination of percentage of immunopositivity per unit area (constant ×200 field). Two-photon microscopy was performed using an Ultima imaging system (Prairie Technologies, Middletown WI), a Ti:sapphire Chameleon Ultra XR femtosecond-pulsed laser (920 nm) (Coherent, Santa Clara, CA), and a 63 × 0.9 NA water-immersion IR objective (Olympus, Center Valley, PA). Stacks of images were reconstructed in 3D using Imaris software (Bitplane, Saint Paul, MN). VEGF mRNA expression levels were determined in cultured cells and xenografts by reverse-transcriptase real-time polymerase chain reaction analysis as described previously (Thompson et al., 2006).

Supplemental Data

The Supplemental Data include six supplemental figures and can be found with this article online at http://www.cancercell.org/cgi/content/full/11/1/69/DC1/.

ACKNOWLEDGMENTS

This work was supported by the Sontag Foundation (R.J.G.), NCI grant CA096832 (R.J.G.), the V-Foundation for Cancer Research (R.J.G.), and the American Lebanese Syrian Associated Charities (ALSAC). We thank the Hartwell Center for Bioinformatics and Biotechnology and the Animal Resource Center at St. Jude Children's Research Hospital.

Received: June 22, 2006
Revised: October 3, 2006
Accepted: November 28, 2006
Published: January 15, 2007

REFERENCES

Aihara, M., Sugawara, K., Torii, S., Hosaka, M., Kurihara, H., Saito, N., and Takeuchi, T. (2004). Angiogenic endothelium-specific nestin expression is enhanced by the first intron of the nestin gene. Lab. Invest. *84*, 1581–1592.

Akita, R.W., and Sliwkowski, M.X. (2003). Preclinical studies with Erlotinib (Tarceva). Semin. Oncol. *30*, 15–24.

Al-Hajj, M., Wicha, M.S., Benito-Hernandez, A., Morrison, S.J., and Clarke, M.F. (2003). From the cover: Prospective identification of tumorigenic breast cancer cells. Proc. Natl. Acad. Sci. USA *100*, 3983–3988.

Bao, S., Wu, Q., Sathornsumetee, S., Hao, Y., Li, Z., Hjelmeland, A.B., Shi, Q., McLendon, R.E., Bigner, D.D., and Rich, J.N. (2006). Stem cell-like glioma cells promote tumor angiogenesis through vascular endothelial growth factor. Cancer Res. *66*, 7843–7848.

Clarke, M.F., and Fuller, M. (2006). Stem cells and cancer: Two faces of eve. Cell *124*, 1111–1115.

De Toni, F., Racaud-Sultan, C., Chicanne, G., Mas, V.M., Cariven, C., Mesange, F., Salles, J.P., Demur, C., Allouche, M., Payrastre, B., et al. (2006). A crosstalk between the Wnt and the adhesion-dependent signaling pathways governs the chemosensitivity of acute myeloid leukemia. Oncogene *25*, 3113–3122.

Dick, J.E., and Lapidot, T. (2005). Biology of normal and acute myeloid leukemia stem cells. Int. J. Hematol. *82*, 389–396.

Erlandsson, A., Larsson, J., and Forsberg-Nilsson, K. (2004). Stem cell factor is a chemoattractant and a survival factor for CNS stem cells. Exp. Cell Res. *301*, 201–210.

Folkerth, R.D. (2004). Histologic measures of angiogenesis in human primary brain tumors. Cancer Treat. Res. *117*, 79–95.

Fuchs, E., Tumbar, T., and Guasch, G. (2004). Socializing with the neighbors: Stem cells and their niche. Cell *116*, 769–778.

Gajjar, A., Hernan, R., Kocak, M., Fuller, C., Lee, Y., McKinnon, P.J., Wallace, D., Lau, C., Chintagumpala, M., Ashley, D.M., et al. (2004). Clinical, histopathologic, and molecular markers of prognosis: Toward a new disease risk stratification system for medulloblastoma. J. Clin. Oncol. *22*, 984–993. Published online February 17, 2004. 10.1200/JCO.2004.06.032.

Galli, R., Binda, E., Orfanelli, U., Cipelletti, B., Gritti, A., De Vitis, S., Fiocco, R., Foroni, C., Dimeco, F., and Vescovi, A. (2004). Isolation and characterization of tumorigenic, stem-like neural precursors from human glioblastoma. Cancer Res. *64*, 7011–7021.

Garcia-Barros, M., Paris, F., Cordon-Cardo, C., Lyden, D., Rafii, S., Haimovitz-Friedman, A., Fuks, Z., and Kolesnick, R. (2003). Tumor response to radiotherapy regulated by endothelial cell apoptosis. Science *300*, 1155–1159.

Hemmati, H.D., Nakano, I., Lazareff, J.A., Masterman-Smith, M., Geschwind, D.H., Bronner-Fraser, M., and Kornblum, H.I. (2003). Cancerous stem cells can arise from pediatric brain tumors. Proc. Natl. Acad. Sci. USA *100*, 15178–15183. Published online November 26, 2003. 10.1073/pnas.2036535100.

Hernan, R., Fasheh, R., Calabrese, C., Frank, A.J., Maclean, K.H., Allard, D., Barraclough, R., and Gilbertson, R.J. (2003). ERBB2 up-regulates S100A4 and several other prometastatic genes in medulloblastoma. Cancer Res. *63*, 140–148.

Jacobsen, P.F., Jenkyn, D.J., and Papadimitriou, J.M. (1985). Establishment of a human medulloblastoma cell line and its heterotransplantation into nude mice. J. Neuropathol. Exp. Neurol. *44*, 472–485.

Jain, R.K., Duda, D.G., Clark, J.W., and Loeffler, J.S. (2006). Lessons from phase III clinical trials on anti-VEGF therapy for cancer. Nat. Clin. Pract. Oncol. *3*, 24–40.

Jin, K., Mao, X.O., Sun, Y., Xie, L., and Greenberg, D.A. (2002). Stem cell factor stimulates neurogenesis in vitro and in vivo. J. Clin. Invest. *110*, 311–319.

Kaplan, R.N., Riba, R.D., Zacharoulis, S., Bramley, A.H., Vincent, L., Costa, C., MacDonald, D.D., Jin, D.K., Shido, K., Kerns, S.A., et al. (2005). VEGFR1-positive haematopoietic bone marrow progenitors initiate the pre-metastatic niche. Nature *438*, 820–827.

Kiel, M.J., Yilmaz, O.H., Iwashita, T., Yilmaz, O.H., Terhorst, C., and Morrison, S.J. (2005). SLAM family receptors distinguish hematopoietic stem and progenitor cells and reveal endothelial niches for stem cells. Cell *121*, 1109–1121.

Kondo, T., Setoguchi, T., and Taga, T. (2004). Persistence of a small subpopulation of cancer stem-like cells in the C6 glioma cell line. Proc. Natl. Acad. Sci. USA *101*, 781–786. Published online January 7, 2004. 10.1073/pnas.0307618100.

Lapidot, T., Sirard, C., Vormoor, J., Murdoch, B., Hoang, T., Caceres-Cortes, J., Minden, M., Paterson, B., Caligiuri, M.A., and Dick, J.E. (1994). A cell initiating human acute myeloid leukaemia after transplantation into SCID mice. Nature *367*, 645–648.

Louissaint, A., Jr., Rao, S., Leventhal, C., and Goldman, S.A. (2002). Coordinated interaction of neurogenesis and angiogenesis in the adult songbird brain. Neuron *34*, 945–960.

Martino, G., and Pluchino, S. (2006). The therapeutic potential of neural stem cells. Nat. Rev. Neurosci. *7*, 395–406.

Moore, K.A., and Lemischka, I.R. (2006). Stem cells and their niches. Science *311*, 1880–1885.

Palmer, T.D., Willhoite, A.R., and Gage, F.H. (2000). Vascular niche for adult hippocampal neurogenesis. J. Comp. Neurol. *425*, 479–494.

Paris, F., Fuks, Z., Kang, A., Capodieci, P., Juan, G., Ehleiter, D., Haimovitz-Friedman, A., Cordon-Cardo, C., and Kolesnick, R. (2001). Endothelial apoptosis as the primary lesion initiating intestinal radiation damage in mice. Science *293*, 293–297.

Phillips, H.S., Kharbanda, S., Chen, R., Forrest, W.F., Soriano, R.H., Wu, T.D., Misra, A., Nigro, J.M., Colman, H., Soroceanu, L., et al. (2006). Molecular subclasses of high-grade glioma predict prognosis, delineate a pattern of disease progression, and resemble stages in neurogenesis. Cancer Cell *9*, 157–173.

Pietsch, T., Scharmann, T., Fonatsch, C., Schmidt, D., Ockler, R., Freihoff, D., Albrecht, S., Wiestler, O.D., Zeltzer, P., and Riehm, H. (1994). Characterization of five new cell lines derived from human primitive neuroectodermal tumors of the central nervous system. Cancer Res. *54*, 3278–3287.

Plate, K.H., Breier, G., Weich, H.A., and Risau, W. (1992). Vascular endothelial growth factor is a potential tumour angiogenesis factor in human gliomas in vivo. Nature *359*, 845–848.

Pumiglia, K., and Temple, S. (2006). PEDF: Bridging neurovascular interactions in the stem cell niche. Nat. Neurosci. *9*, 299–300.

Quinones-Hinojosa, A., Sanai, N., Soriano-Navarro, M., Gonzalez-Perez, O., Mirzadeh, Z., Gil-Perotin, S., Romero-Rodriguez, R., Berger, M.S., Garcia-Verdugo, J.M., and Alvarez-Buylla, A. (2006). Cellular composition and cytoarchitecture of the adult human subventricular zone: A niche of neural stem cells. J. Comp. Neurol. *494*, 415–434.

Ramirez-Castillejo, C., Sanchez-Sanchez, F., Andreu-Agullo, C., Ferron, S.R., Aroca-Aguilar, J.D., Sanchez, P., Mira, H., Escribano, J., and Farinas, I. (2006). Pigment epithelium-derived factor is a niche signal for neural stem cell renewal. Nat. Neurosci. *9*, 331–339. Published online February 19, 2006. 10.1038/nn1657.

Reardon, D.A., and Wen, P.Y. (2006). Therapeutic advances in the treatment of glioblastoma: Rationale and potential role of targeted agents. Oncologist *11*, 152–164.

Sanai, N., Tramontin, A.D., Quinones-Hinojosa, A., Barbaro, N.M., Gupta, N., Kunwar, S., Lawton, M.T., McDermott, M.W., Parsa, A.T., Manuel-Garcia Verdugo, J., et al. (2004). Unique astrocyte ribbon in adult human brain contains neural stem cells but lacks chain migration. Nature *427*, 740–744.

Sanai, N., Alvarez-Buylla, A., and Berger, M.S. (2005). Neural stem cells and the origin of gliomas. N. Engl. J. Med. *353*, 811–822.

Saucier, C., Khoury, H., Lai, K.M., Peschard, P., Dankort, D., Naujokas, M.A., Holash, J., Yancopoulos, G.D., Muller, W.J., Pawson, T., and Park, M. (2004). The Shc adaptor protein is critical for VEGF induction by Met/HGF and ErbB2 receptors and for early onset of tumor angiogenesis. Proc. Natl. Acad. Sci. USA *101*, 2345–2350.

Shen, Q., Goderie, S.K., Jin, L., Karanth, N., Sun, Y., Abramova, N., Vincent, P., Pumiglia, K., and Temple, S. (2004). Endothelial cells stimulate self-renewal and expand neurogenesis of neural stem cells. Science *304*, 1338–1340. Published online April 1, 2004. 10.1126/science.1095505.

Singh, S.K., Hawkins, C., Clarke, I.D., Squire, J.A., Bayani, J., Hide, T., Henkelman, R.M., Cusimano, M.D., and Dirks, P.B. (2004). Identification of human brain tumour initiating cells. Nature *432*, 396–401.

Sipkins, D.A., Wei, X., Wu, J.W., Runnels, J.M., Cote, D., Means, T.K., Luster, A.D., Scadden, D.T., and Lin, C.P. (2005). In vivo imaging of specialized bone marrow endothelial microdomains for tumour engraftment. Nature *435*, 969–973.

Sun, L., Hui, A.-M., Su, Q., Vortmeyer, A., Kotliarov, Y., Pastorino, S., Passaniti, A., Menon, J., Walling, J., Bailey, R., et al. (2006). Neuronal and glioma-derived stem cell factor induces angiogenesis within the brain. Cancer Cell *9*, 287–300.

Taylor, M.D., Poppleton, H., Fuller, C., Su, X., Liu, Y., Jensen, P., Magdaleno, S., Dalton, J., Calabrese, C., Board, J., et al. (2005). Radial glia cells are candidate stem cells of ependymoma. Cancer Cell *8*, 323–335.

Thompson, M.C., Fuller, C., Hogg, T.L., Dalton, J., Finkelstein, D., Lau, C.C., Chintagumpala, M., Adesina, A., Ashley, D.M., Kellie, S.J., et al. (2006). Genomics identifies medulloblastoma subgroups that are enriched for specific genetic alterations. J. Clin. Oncol. *24*, 1924–1931. Published online March 27, 2006. 10.1200/JCO.2005.04.4974.

Uchida, N., Buck, D.W., He, D., Reitsma, M.J., Masek, M., Phan, T.V., Tsukamoto, A.S., Gage, F.H., and Weissman, I.L. (2000). Direct isolation of human central nervous system stem cells. Proc. Natl. Acad. Sci. USA *97*, 14720–14725.

Wada, T., Haigh, J.J., Ema, M., Hitoshi, S., Chaddah, R., Rossant, J., Nagy, A., and van der Kooy, D. (2006). Vascular endothelial growth factor directly inhibits primitive neural stem cell survival but promotes definitive neural stem cell survival. J. Neurosci. *26*, 6803–6812.

Wodarz, A., and Gonzalez, C. (2006). Connecting cancer to the asymmetric division of stem cells. Cell *124*, 1121–1123.

Wurmser, A.E., Palmer, T.D., and Gage, F.H. (2004). Neuroscience. Cellular interactions in the stem cell niche. Science *304*, 1253–1255.

Yilmaz, O.H., Valdez, R., Theisen, B.K., Guo, W., Ferguson, D.O., Wu, H., and Morrison, S.J. (2006). Pten dependence distinguishes haematopoietic stem cells from leukaemia-initiating cells. Nature *441*, 475–482.